2-25-2015

The Mps1 Kinase Modulates the Recruitment and Activity of Cnn1CENP-T at Saccharomyces cerevisiae Kinetochores

Kriti Shrestha Thapa
Purdue University

Amanda Oldani
Istituto FIRC di Oncologia Molecolare

Cinzia Pagliuca
European Institute of Oncology

Peter De Wulf
European Institute of Oncology

Tony R. Hazbun
Purdue University, thazbun@purdue.edu

Recommended Citation

Thapa KS, Oldani A, Pagliuca C, De Wulf P, Hazbun TR. The Mps1 kinase modulates the recruitment and activity of Cnn1(CENP-T) at Saccharomyces cerevisiae kinetochores. Genetics. 2015 May;200(1):79-90. doi: 10.1534/genetics.115.175786. Epub 2015 Feb 25. PMID: 25716979; PMCID: PMC4423383.

The Mps1 Kinase Modulates the Recruitment and Activity of Cnn1^{CENP-T} at *Saccharomyces cerevisiae* Kinetochores

Kriti Shrestha Thapa,* Amanda Oldani,† Cinzia Pagliuca,‡ Peter De Wulf,‡ and Tony R. Hazbun*,[1]

*Purdue University, Department of Medicinal Chemistry and Molecular Pharmacology, Purdue University Center for Cancer Research, West Lafayette, Indiana 47907-2091, †Istituto FIRC (Fondazione Italiana per la Ricerca sul Cancro) di Oncologia Molecolare, 20139 Milan, Italy, and ‡European Institute of Oncology, Department of Experimental Oncology, 20139 Milan, Italy

ORCID IDs: 0000-0001-9772-5881 (P.D.W); 000-0003-0675-8093 (T.R.H).

ABSTRACT Kinetochores are conserved protein complexes that bind the replicated chromosomes to the mitotic spindle and then direct their segregation. To better comprehend *Saccharomyces cerevisiae* kinetochore function, we dissected the phospho-regulated dynamic interaction between conserved kinetochore protein Cnn1^{CENP-T}, the centromere region, and the Ndc80 complex through the cell cycle. Cnn1 localizes to kinetochores at basal levels from G1 through metaphase but accumulates abruptly at anaphase onset. How Cnn1 is recruited and which activities regulate its dynamic localization are unclear. We show that Cnn1 harbors two kinetochore-localization activities: a C-terminal histone-fold domain (HFD) that associates with the centromere region and a N-terminal Spc24/Spc25 interaction sequence that mediates linkage to the microtubule-binding Ndc80 complex. We demonstrate that the established Ndc80 binding site in the N terminus of Cnn1, Cnn1$^{60–84}$, should be extended with flanking residues, Cnn1$^{25–91}$, to allow near maximal binding affinity to Ndc80. Cnn1 localization was proposed to depend on Mps1 kinase activity at Cnn1–S74, based on *in vitro* experiments demonstrating the Cnn1–Ndc80 complex interaction. We demonstrate that from G1 through metaphase, Cnn1 localizes via both its HFD and N-terminal Spc24/Spc25 interaction sequence, and deletion or mutation of either region results in anomalous Cnn1 kinetochore levels. At anaphase onset (when Mps1 activity decreases) Cnn1 becomes enriched mainly via the N-terminal Spc24/Spc25 interaction sequence. In sum, we provide the first *in vivo* evidence of Cnn1 preanaphase linkages with the kinetochore and enrichment of the linkages during anaphase.

KEYWORDS Cnn1; Mps1; kinetochore; centromere; CENP-T

KINETOCHORES are large protein structures that assemble hierarchically on the centromeres (*CEN*) of replicated chromosomes (sister chromatids). They biorient each sister chromatid pair to the microtubules (MTs) of the mitotic spindle and orchestrate chromatid segregation into the daughter cells (Cheeseman 2014; Malvezzi and Westermann 2014). At the core of each kinetochore lies a protein network named KMN (**K**LN1/Spc105, **M**IS12/Mtw1, and **N**DC80/Ndc80 complexes) that bridges the *CEN* and MTs (Cheeseman *et al.* 2006; Westermann *et al.* 2007). The Ndc80 complex attaches kinetochores to the MTs via its outer Ndc80/Nuf2 dimer (Wei *et al.* 2007; Ciferri *et al.* 2008; Alushin *et al.* 2010), while its *CEN*-proximal Spc24/Spc25 dimer interacts with a putatively *CEN*-associated protein, known as Cnn1 in budding yeast (CENP-T in metazoans). The N-terminal domain of Cnn1 and CENP-T hook onto the interface of the Spc24/Spc25 dimer (Malvezzi *et al.* 2013; Nishino *et al.* 2013). In its C terminus, Cnn1 harbors a histonefold domain (HFD) (Schleiffer *et al.* 2012), which may associate with *CEN* DNA, as does CENP-T (Hori *et al.* 2008; Nishino *et al.* 2012).

Cnn1 levels at kinetochores are low from G1 through metaphase but increase two- to threefold at anaphase entry and drop back to base level at anaphase exit. Cnn1 interacts with the Ndc80 complex via its N-terminal domain and is thought to be unbound during interphase as the Ndc80 complex is associated with the Mtw1 complex. Cnn1's phosphorylation

doi: 10.1534/genetics.115.175786
Manuscript received November 11, 2014; accepted for publication February 24, 2015; published Early Online February 25, 2015.
Supporting information is available online at http://www.genetics.org/lookup/suppl/doi:10.1534/genetics.115.175786/-/DC1.
[1]Corresponding author: 575 Stadium Mall Dr., West Lafayette, IN 47907. E-mail: thazbun@purdue.edu

state reflects its recruitment profile to kinetochores (Bock *et al.* 2012) and mirrors that of Mps1 kinase activity (Palframan *et al.* 2006). Indeed, altering Mps1 expression indicated its involvement in Cnn1 phosphorylation (Malvezzi *et al.* 2013) and possibly localization at kinetochores. Mps1 targets Cnn1 *in vitro* at several sites (Bock *et al.* 2012; Malvezzi *et al.* 2013) and its activity inhibits the interaction between Cnn1 and the Ndc80 complex, both *in vitro* and in yeast (Malvezzi *et al.* 2013).

Cnn1 also interacts with the $Cdc28^{Cdk1}$ kinase in yeast (Breitkreutz *et al.* 2010). Recombinant Cnn1 was phosphorylated *in vitro* by Cdc28 as well as by the Ipl1 kinase (Cheeseman *et al.* 2002; De Wulf *et al.* 2009; Breitkreutz *et al.* 2010; Bock *et al.* 2012; Malvezzi *et al.* 2013). As such, a complex but minimally understood phospho-regulatory network acts on Cnn1 with unknown physiological roles and relative contributions from the involved kinases.

Here, we show that the Mps1 kinase controls Cnn1 localization and activity at kinetochores through the cell cycle. Two domains mediate kinetochore recruitment of Cnn1: the C-terminal HFD binds to the *CEN* region, whereas the N-terminal domain allows recruitment via the Ndc80 complex. Mps1 dictates the domain used by targeting one residue, S74. S74 is located within a short N-terminal domain sequence we delineate as the Spc24/Spc25 **i**nteraction **s**equence (SIS) via which Cnn1 binds to the Ndc80 complex with maximal affinity. SIS-mediated recruitment is restrained by Mps1 activity increasing through metaphase but additional factors in addition to S74 phosphorylation must affect recruitment. At anaphase onset, Cnn1 abruptly accumulates at kinetochores mostly via the SIS due to reduced S74 phosphorylation by Mps1.

Materials and Methods

Protein purification

Various *GST–CNN1* constructs, *GST–SPC24* and *GST–SPC25* (globular domain residues 128–222) were cloned into pGEX-6P-1 (GE Healthcare Life Sciences) and transformed into *Escherichia coli* BL21–DE3. Cells were induced with 0.2–1 mM isopropyl β-D-1-thiogalactopyranoside (IPTG) (4 hr at 30° or overnight at 25°) and lysed by sonication or via use of bacterial protein extraction reagent (B-PER). Cell lysates were incubated with glutathione agarose beads (Thermo Scientific) and the proteins were eluted with 10 mM reduced glutathione (Thermo Scientific; Sigma) in 50 mM Tris buffer, pH 8.0. The protein concentrations were measured using the Micro BCA Protein Assay kit (Thermo Scientific) and the purity was determined using SDS–polyacrylamide gel electrophoresis (PAGE) and Coomassie staining.

His6–$CNN1^{1–150}$ was cloned into pET28b (EMD Bioscience). *His6–*$CNN1^{1–150}$*–S74A*, *His6–*$CNN1^{1–150}$*–S74D*, and *His6–*$CNN1^{1–150}$*–T91D* were generated using single-site mutagenesis. Following induction with 1 mM IPTG for 3 hr at 37°, proteins were eluted with 50 mM Tris, pH 8.0, 250 mM imidazole, and 0.3 M NaCl from HIS select Nickel affinity gel (Sigma). Similarly, His6–Spc24/Spc25 was induced with 0.5 M IPTG overnight at 18° and eluted with 50 mM Tris, pH 8.0, 250 mM imidazole, and 150 mM NaCl from HIS select Nickel affinity gel (Sigma).

Interaction analysis

Native PAGE and SDS–PAGE were performed using 4–15% Mini-Protean TGX precast Gels (Biorad). Protein samples were mixed at equimolar concentration (4 μM), and incubated on ice for 1 hr and analyzed under native condition at 150 V for 4 hr at 4° or under denaturing condition at 150 V for 1 hr at room temperature. For Western blot analysis of the native PAGE gels, 1.5 μM BSA was supplemented to all protein mixtures (1 μM) before incubation on ice. The gels were stained using GelCode Blue (Thermo Scientific).

To screen the protein–protein interactions using yeast two-hybrid analysis, all the Cnn1 (S/T) mutations were generated via site-directed mutagenesis and verified by sequencing. PJ69-4a was used as the reporter strain (James *et al.* 1996). Nuf2, Spc24, and Spc25 were expressed as fusion proteins with the Gal4 DNA-binding domain in PJ694. All Cnn1 mutants were expressed as fusion proteins with the Gal4 activation domain. Yeast two-hybrid was performed as previously described to analyze for the ability to grow as a consequence of *HIS3* transcription using medium lacking tryptophan, leucine and histidine (SD −TLH) in addition to 3 mM or 10 mM aminotriazole (Wong *et al.* 2007).

Western blot

To verify the complex formation in native PAGE gels, proteins were identified using 1:1000 dilution of mouse monoclonal anti-GST (GeneCopoeia) antibody and 1:10,000 dilution of secondary antimouse HRP-conjugated antibody (GE Healthcare).

To determine protein expression, yeast proteins were separated under denaturing conditions followed by Western blotting. Cnn1 fused to green fluorescent protein (GFP) (Cnn1–GFP) and its mutants were identified by 1:500 dilution of mouse monoclonal anti-GFP (Roche) antibody and 1:10,000 dilution of secondary antimouse HRP-conjugated antibody (GE Healthcare).

Biolayer interferometry binding measurements

The binding measurements were analyzed using either the BLItz or OctetRed96 system from ForteBio. To measure binding affinity, 20–25 μg/ml of His6- or GST-tagged proteins were immobilized on Ni-NTA or GST biosensor tips, respectively. After equilibration, the tips were probed with the interacting partners (analytes) at varying concentrations depending on the expected K_d for 5 min. The complexes were dissociated by immersing the sensor into sample dilution buffer (ForteBio) for 5 min. The binding affinities were derived using the BLItz Pro software and Octet software and the graphs were plotted using GraphPad Prism (GraphPad).

Sequence alignment and modeling

Budding yeast Cnn1 orthologs (www.yeastgenome.org) were aligned with Muscle (Edgar 2004). Each residue in the alignment was assigned a color, depending on the residue type

and frequency of its occurrence in the column (Thompson *et al.* 1997). The Cnn1 images were generated using the Protein Data Bank (PDB) coordinates file (entry 4GEQ) (Malvezzi *et al.* 2013). The Cnn1 PDB model consists of the Spc24 C-terminal domain (residues 155–213) and Spc25 C-terminal domain (residues 133–221) with the Cnn1 N-terminal motif (residues 60–84). To generate the 3D model of the *Candida glabrata* Cnn1–Spc24/Spc25 complex, we modeled the *C. glabrata* Spc24/Spc25 sequences with Modeler (Eswar *et al.* 2006) using the *Saccharomyces cerevisiae* Spc24/Spc25 crystal structure as the reference. We then added the Cnn1 peptide by changing the residues of the *S. cerevisiae* Cnn1 peptide into those of *C. glabrata* (see alignment in Figure 1A). All figures were prepared with PyMOL (The PyMOL Molecular Graphics System, Schrödinger).

Fluorescence microscopy

Cells for fluorescence imaging were grown in complete synthetic medium at 23°. Imaging was performed on a DeltaVision Elite deconvolution system (Applied Precision) controlled by softWoRx software (Applied Precision) equipped with a CoolSNAP HQ2 CCD camera (Photometrics) and an IX71 Olympus inverted microscope using a ×100 oil-immersion objective (UPLS Apochromat ×100 N.A. 1.4; Olympus). The system was equipped with an environmental chamber (Applied Precision) maintained at 23°. Images were acquired as Z stacks (1 × 1 binning, XY image dimensions: 1024 × 1024, 17 sections of 0.3 μm), deconvolved and projected down the Z-axis with maximal intensity. The background subtracted, and the signals were quantified with ImageJ64 (National Institutes of Health). Cnn1 fluorescence levels at the kinetochore were expressed as a ratio of the GFP signal to the spindle pole Spc110–mCherry reference signal.

Cells expressing $Cnn1^{1–150}$–GFP from a P_{GAL1} plasmid and endogenously expressing Spc110–mCherry were grown in 2% raffinose synthetic medium lacking tryptophan at 30°. Kinetochore clusters were observed using a Nikon AR1 confocal microscope with ×60 (N.A. 1.49) oil-immersion objective. All of the images were acquired as *Z* stacks (13 sections of 0.3 μm) and processed using the Nikon elements software with a maximum *Z* projection.

Yeast strains and serial dilution growth assay

All yeast cells have a W303a background unless stated otherwise and are listed in Supporting Information, Table S1. *Cnn1–GFP* strains (27-residue linker between Cnn1 and GFP) were constructed using an integrative vector (pRS306) (Sikorski and Hieter 1989) that was recombined at the *CNN1* promoter in *cnn1Δ Spc110–mCherry* and *cnn1Δ nnf1–17* strains. *Cnn1–S74A* and *Cnn1–S74D* were created using site-directed mutagenesis and recombined in a similar fashion. $Cnn1^{\Delta HFD}$ was created using polymerase chain reaction (PCR)-mediated deletion as described (Hansson *et al.* 2008). $Cnn1^{\Delta HFD}$–*S74A* and $Cnn1^{\Delta HFD}$–*S74D* were created using site-directed mutagenesis and recombined described as above.

An expression vector expressing $Cnn1^{1–150}$–GFP was constructed into the pAG414–GAL–ccdB–EGFP plasmid by Gateway cloning with an intervening linker from plasmid pOBD2. This linker encodes the first 74 residues of the Gal4 DNA-binding domain including a nuclear localization sequence.

Various Cnn1 constructs were overexpressed from the $P_{GAL1/10}$ promoter (pESC −ura vector) in W303, *cnn1Δ Spc110–mCherry*, or *cnn1Δ nnf1–17* strains. For serial growth dilution assays, temperature-sensitive strains were grown at permissive temperature overnight in synthetic medium lacking uracil (CSM −Ura (Sunrise Science) with 2% raffinose (Affymetrix). The overnight cultures were diluted to OD_{600} = 0.6 and fivefold serial dilutions were spotted onto synthetic agar medium lacking uracil with 2% raffinose and 2% galactose (Affymetrix) and incubated at 25° (permissive), 30° (semi-permissive) and 32°–33° (nonpermissive) for at least 2 days. We found that 33° allowed growth of the *cnn1Δ nnf1–17* strain with 2% glucose in 3 days, whereas 37° did not. Synthetic medium lacking uracil with 2% glucose (suppressed expression) was used as control plates. For integrated strains, the dilution assay was conducted using YP 2% glucose agar medium instead of synthetic medium.

Plasmids

All the plasmids used in this study are listed in Table S2. All the *CNN1* mutants were created using site-directed mutagenesis.

Results

Cnn1 binds to Spc24/Spc25 via a conserved motif comprising residues 25–91

The first 150 residues of Cnn1 ($Cnn1^{1–150}$) bound to Spc24/Spc25 *in vitro* and in yeast two-hybrid studies (Bock *et al.* 2012; Schleiffer *et al.* 2012). A conserved 15-residue motif ($Cnn1^{65–79}$) was previously found to be sufficient to mediate Spc24/Spc25 binding (Schleiffer *et al.* 2012). The binding constant (K_d) for Spc24/Spc25 of a similar fragment ($Cnn1^{60–84}$), established by isothermal titration calorimetry at 3.50 μM, was ∼200-fold lower as compared to Cnn1 lacking its C-terminal HFD ($Cnn1^{\Delta HFD}$, 0.016 μM) (Malvezzi *et al.* 2013). A conserved candidate-binding motif in the N terminus of Cnn1 (residues 130–166) only slightly affected the binding affinity of Cnn1 (Malvezzi *et al.* 2013). In addition, deletion of $Cnn1^{91–125}$ did not affect plasmid segregation (Malvezzi *et al.* 2013). Hence, residues toward the N-terminal region of $Cnn1^{65–79}$ might be better positioned to stabilize the Spc24/Spc25 contact. The N-terminal region of Cnn1 is conserved between *S. cerevisiae* and related fungi and harbors three putative α-helices: 23–40, 65–79, and 90–100 (Figure 1A, Figure S1). Guided by the predicted 2D structure of Cnn1, we probed by native PAGE a set of N-terminal fragments for their ability to form a complex with Spc24/Spc25 (Figure 1B). Four fragments bound to Spc24/Spc25: 1–150, 25–91, 47–91, and 60–91. Western blot analysis confirmed the presence of these Cnn1 fragments fused to GST in the slow-migrating complexes (Figure 1C). We measured their affinities for Spc24/Spc25

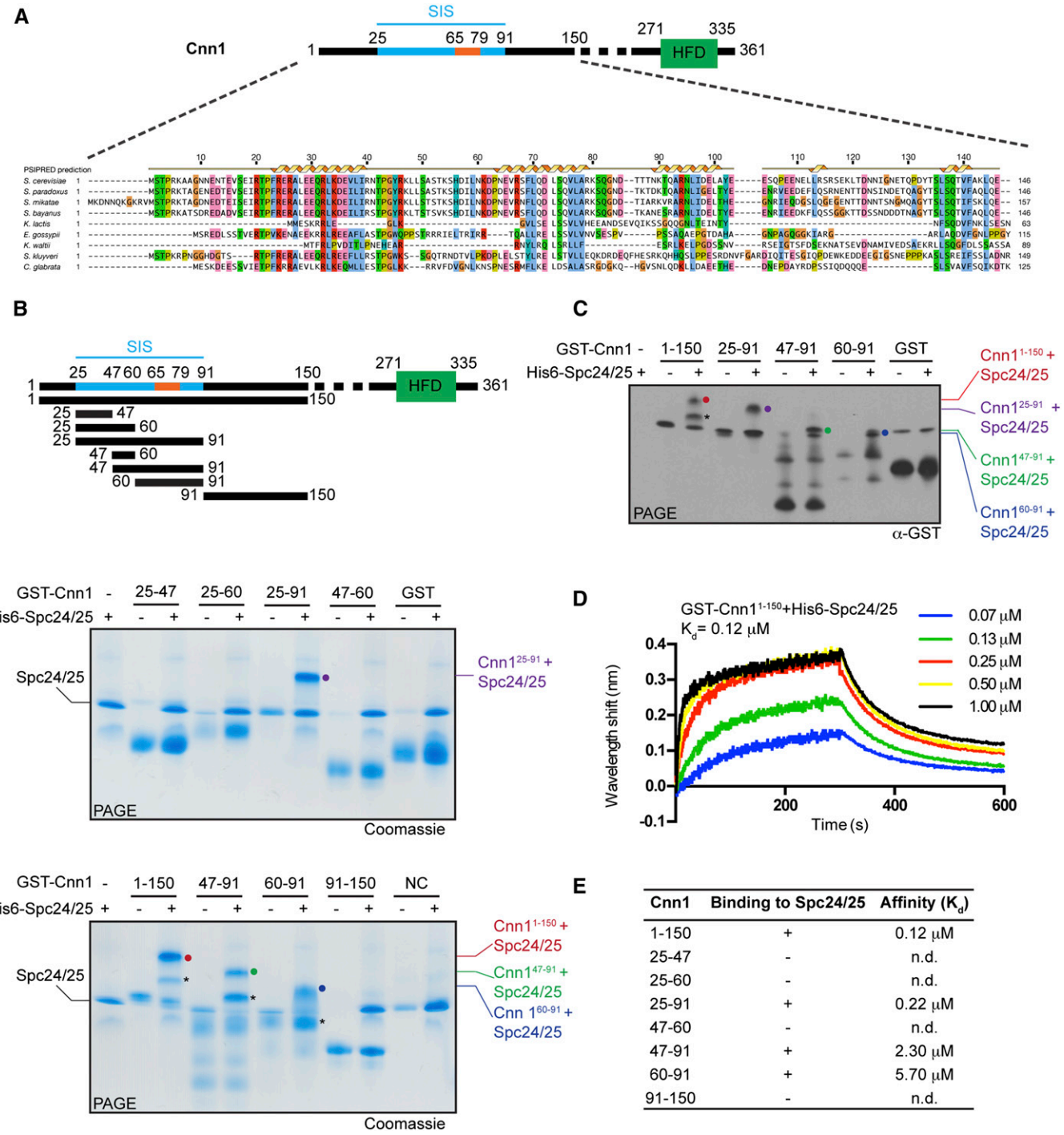

E

Cnn1	Binding to Spc24/25	Affinity (K_d)
1-150	+	0.12 μM
25-47	-	n.d.
25-60	-	n.d.
25-91	+	0.22 μM
47-60	-	n.d.
47-91	+	2.30 μM
60-91	+	5.70 μM
91-150	-	n.d.

Figure 1 SIS is essential for a stable interaction with Spc24/Spc25. (A) Sequence alignment of Cnn1$^{1–150}$ with other fungal species. Blue, SIS (Spc24/Spc25 **i**nteraction **s**equence); orange, conserved motif. (B) Schematic outline of Cnn1 N-terminal fragments expressed as GST fusion proteins (top). Native PAGE of GST–Cnn1 fragment interactions with His6–Spc24/Spc25 (4 μM) (middle and bottom). Negative control (NC), unrelated GST-fusion protein; circle, complexed protein; asterisk, truncated form of the complex. Note that the negative control migration pattern is similar to His6–Spc24/Spc25. (C) Western blot of native PAGE with GST–Cnn1–His6–Spc24/Spc25 complexes from B (1 μM). (D) Biolayer interferometry binding measurement of GST–Cnn1$^{1–150}$ and His6–Spc24/Spc25 as analyte at varying concentrations (0 μM, 0.07 μM, 0.13 μM, 0.25 μM, 0.50 μM, and 1 μM). (E) Affinity of GST–Cnn1 fragments for His6–Spc24/Spc25 measured with biolayer interferometry (N.D., not determined).

via biolayer interferometry analysis and found that only the K_d of Cnn1$^{25–91}$ (0.22 μM) approached that of Cnn1$^{1–150}$ (0.12 μM) (Figure 1, D and E). A discrepancy of binding affinity was observed for Cnn1$^{1–150}$ (0.12 μM) compared to the Cnn1$^{\Delta HFD}$ fragment (0.016 μM) (Malvezzi *et al.* 2013) possibly due to a shorter Cnn1 fragment than the Cnn1$^{\Delta HFD}$ fragment together

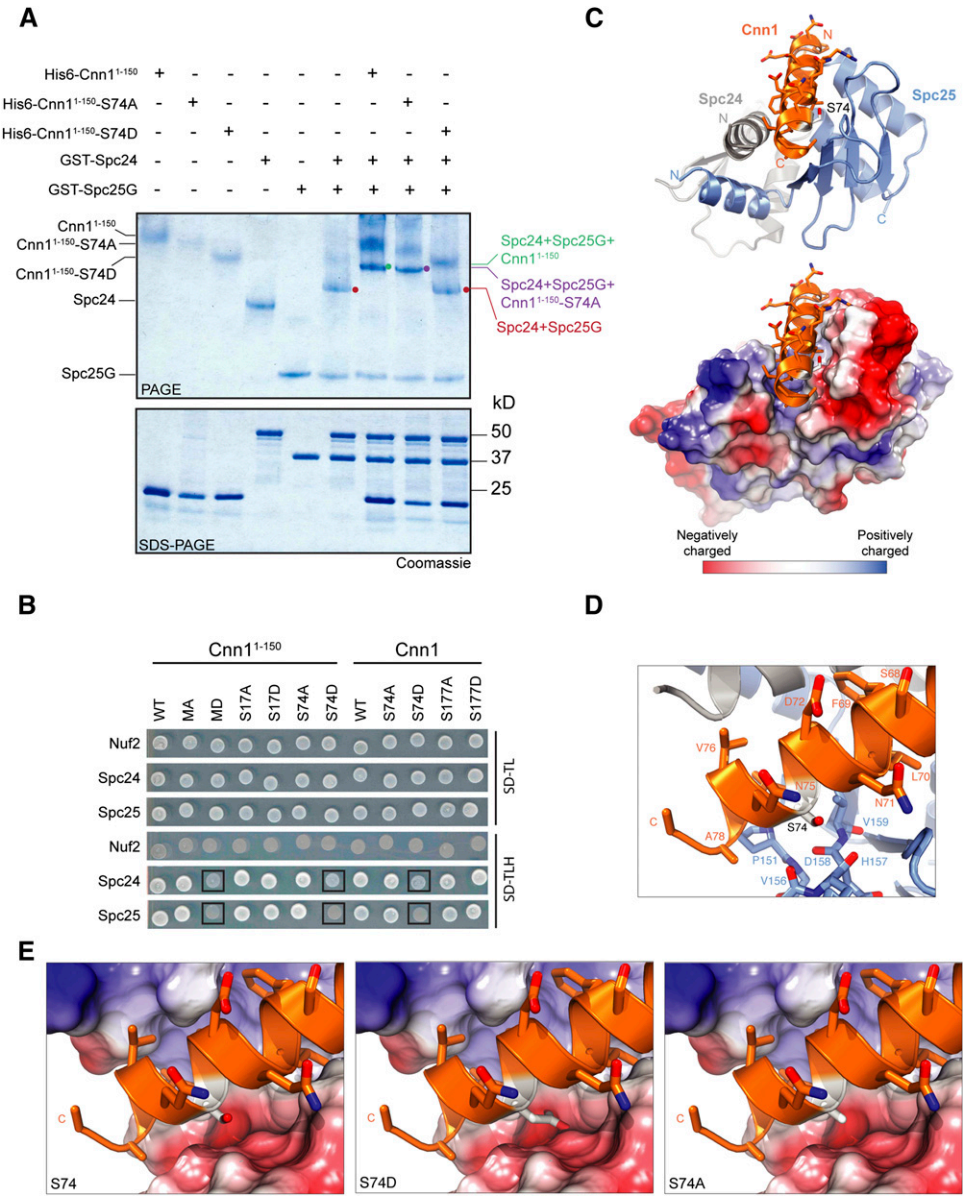

Figure 2 Phosphomimetic substitution of Cnn1–S74 negatively regulates its association with Spc24/Spc25. (A) His6–Cnn1$^{1–150}$, His6–Cnn1$^{1–150}$–S74A, and His6–Cnn1$^{1–150}$–S74D were incubated with GST–Spc24 and GST–Spc25G (4 μM) and analyzed by native PAGE (top) and SDS–PAGE (bottom). (B) Cnn1–S74D eliminates the interaction with Spc24/Spc25 as shown by yeast two hybrid. MA and MD are Mps1 sites (T14, S17, T21, and S74) mutated to alanine or aspartic acid, respectively. Nuf2, negative control; SD −TL, synthetic dextrose medium deficient in tryptophan and leucine; SD −TLH, synthetic dextrose medium deficient in tryptophan, leucine, and histidine; black box, no growth. (C) Crystal structure of Cnn1$^{60–84}$ in complex with Spc24/Spc25 generated from PDB file (4GEQ). Spc24 C-terminal domain (residues 155–213) and Spc25 C-terminal domain (residues 133–221) are depicted. (D) View of Cnn1–S74 positioned within a pocket formed by Spc25 residues. (E) Cnn1–S74D substitution projects into a negatively charged environment but S74 and S74A do not.

with use of different methods. Although flanking residues 25–47 proved incapable of interacting with Spc24/Spc25 (Figure 1B) they promoted the affinity of Cnn1$^{65–79}$ for Spc24/Spc25. In conclusion, our data show that although the main binding fragment is Cnn1$^{65–79}$ (Schleiffer *et al.* 2012), additional residues that are not directly involved in Spc24/Spc25 recognition enhance the interaction between Spc24/Spc25 and the core Cnn1$^{25–91}$ binding fragment, which we designate as the SIS peptide.

Mps1 activity at S74 inhibits SIS– Spc24/Spc25 binding

In vitro experiments revealed that S74, which resides centrally in SIS (second α-helix) and is conserved among most budding yeasts (Figure 1A) (Schleiffer *et al.* 2012), is an Mps1 target directly involved in the regulation of Cnn1–Spc24/Spc25 binding (Bock *et al.* 2012; Schleiffer *et al.* 2012; Malvezzi *et al.* 2013). A phosphomimetic substitution (S74D) inhibited Cnn1–Spc24/Spc25 binding in yeast and reduced minichromosome stability, whereas a phospho-null variant (S74A) did not affect Cnn1–Spc24/Spc25 binding nor Cnn1 recruitment to kinetochores (Schleiffer *et al.* 2012; Malvezzi *et al.* 2013). To understand the functional implications of these observations, we first made S74D and S74A versions of Cnn1$^{1–150}$ and compared their affinity for Spc24 and Spc25G (Spc25 globular domain residues 128–222). Cnn1$^{1–150}$ and Cnn1$^{1–150}$–S74A formed slow-migrating complexes with Spc24 and Spc25G with a similar K_d (0.12 μM), whereas Cnn1$^{1–150}$–S74D did not (Figure 2A), indicating that phosphorylation of Cnn1 at S74 inhibits the interaction. Yeast two-hybrid analyses confirmed these findings (Figure 2B). As Cnn1 harbors nine additional known or putative Mps1 target residues in the N-terminal

Table 1 Summary of phosphorylation sites tested in Cnn1

Mutations	Kinase[a]	Interaction with Spc24/Spc25	
		Yeast two hybrid	Native gel
S74A	Mps1	+	+
S74D	Mps1	–	–
S17A	Mps1	+	N.D.
S17D	Mps1	+	N.D.
S177A	Mps1/Cdc28	+	N.D.
S177D	Mps1/Cdc28	+	N.D.
T14A, S17A, T21A, and S74A	Mps1	+	N.D.
T14D, S17D, T21D, and S74D	Mps1	–	N.D.
T53D	Mps1	+	N.D.
T86D	Mps1	+	N.D.
T91D	Mps1	N.D.	+
S268A and S269A	Ipl1	+	N.D.
S268D and S269D	Ipl1	+	N.D.
T3A	Cdc28	+	N.D.
T3D	Cdc28	+	N.D.
T21A	Cdc28/Mps1	+	N.D.
T21D	Cdc28/Mps1	+	N.D.
T42A, S81A, and T121A	Cdc28 (T42)/other S/T[b]	+	N.D.
T42D, S81D, and T121D	Cdc28 (T42)/other S/T[b]	+	N.D.

N.D., not determined (Mps1 sites: T88, T134, S135, T139, S153, and T174).
[a] Kinase sites based on experimental evidence or because of a consensus sequence suggesting a possible kinase site (Bock *et al.* 2012; Schleiffer *et al.* 2012; Malvezzi *et al.* 2013).
[b] Other S/T, random serines or threonines that have no evidence of phosphorylation.

domain, we probed whether their phospho states affect Spc24/Spc25 binding. In addition, we examined residues targeted by Ipl1 and Cdc28 *in vitro*, as well as nearby serine or threonine sites. Yeast two-hybrid and/or native PAGE experiments showed that of all residues tested singly or in combination, only one, S74, controls Cnn1–Spc24/Spc25 binding (Table 1). The crystal structure of the $Cnn1^{60–84}$ peptide in complex with Spc24/Spc25 indicates that Cnn1–S74 binds to a hydrophobic pocket in Spc25, as noted previously by Malvezzi *et al.* (2013) (Figure 2, C and D). However, we add to the previous observations of the co-crystal structure by noting that Mps1 could access the S74 residue even when Cnn1 is bound to Spc24/Spc25 and hence could initiate dissociation of the complex (Figure 2E). We also model the S74A and S74D mutations and show that the aspartic acid substitution would have decreased affinity because it projects into the negatively charged environment partly contributed by D158 (Figure 2, D and E).

Our alignment of Cnn1 revealed that S74 is conserved among most budding yeasts, except for *C. glabrata* (Figure 1A). Indeed, Cnn1–S74 corresponds to D63 in *C. glabrata* Cnn1. To examine how this negatively charged residue may affect binding to Spc24/Spc25, we computationally modeled the Cnn1–Spc24/Spc25 interaction in *C. glabrata*. We find that the local environment of Spc24/Spc25 is positively charged in the *C. glabrata* (K60, K160, H164) and negatively in *S. cerevisiae* (Figure 2E, Figure S2). As such, D63 will positively interact with basic residues in Spc24/Spc25. S64 in *C. glabrata* appears to be accessible for phosphorylation, which could strengthen the positive interaction with Spc24/Spc25, similar to mammalian Spc24/Spc25 in which phosphorylation (by CDK1) promotes Cnn1–Spc24/Spc25 binding.

Synthetic genetic analysis of Cnn1 domains and their regulation by Mps1

Yeast *cnn1Δ* mutants suffer from enhanced chromosome loss but do not exhibit reduced fitness (Bock *et al.* 2012). Consistent with this, expressing *CNN1–S74A*, *CNN1–S74D*, or $CNN1^{\Delta HFD}$ from the endogenous *CNN1* promoter in a *cnn1Δ* strain did not reveal any reduction in viability (Figure 3A). In contrast, expressing *CNN1* from the galactose-inducible and glucose-repressible P_{GAL} promoter on a multicopy plasmid results in lethality (Bock *et al.* 2012) (Figure 3B, Figure S3). Overexpressing full-length Cnn1 and Cnn1 fragments containing the SIS (1–91, 1–150) or their S74A variants caused lethality, but the S74D variants did not, indicating the latter do not interact with the Ndc80 complex. Overexpressing the HFD alone ($Cnn1^{271–335}$) was not lethal demonstrating that the SIS–Ndc80 complex interaction is sufficient to cause lethality.

The high-temperature-sensitive *nnf1-17* kinetochore mutant exhibits moderate growth at slightly elevated temperature (32°), dies at 37°, and has further reduced growth when Cnn1 is deleted (*cnn1Δ*) (Bock *et al.* 2012). As such, expressing Cnn1, Cnn1 domain fragments, or S74 variants in the *cnn1Δ nnf1–17* strain indicates whether the proteins are functional, which was confirmed for Cnn1, Cnn1–S74A, and Cnn1–S74D (Figure 4A). The Cnn1–S74D should not interact with the Ndc80 complex, but does rescue the *cnn1Δ nnf1–17* strain, likely because of the contribution from the HFD. Indeed, genes lacking the HFD were not able to rescue growth (Figure 4A). Interestingly, overexpressing only the HFD completely rescued viability, consistent with our above synthetic genetic interaction studies with the HFD and the *nnf1–17* kinetochore mutant strain (Figures 4B, Figure S4).

Cnn1 recruitment via HFD and/or SIS is dictated by Mps1

To translate our biochemical and genetic data into a functional model, we imaged GFP-tagged Cnn1, $Cnn1^{\Delta HFD}$, and the corresponding S74A and S74D variants at various cycle stages. These constructs allowed us to quantitatively discriminate between the contributions of the HFD and SIS in Cnn1 recruitment (Spc110–mCherry fluorescence levels acted as the reference). Cnn1–GFP localized to kinetochores from G1 through metaphase and became enriched two- to threefold at anaphase entry (21.43% of metaphase cells had an intensity ratio of 2.5 or greater compared to 53.03% of anaphase cells) (Figure 5, A and B; Table S3) (Bock *et al.* 2012). In contrast, the S74A and S74D strains differed in that the signal did not increase markedly from metaphase to anaphase, indicating a disrupted regulation of this transition. Signals increased gradually in every phase from G1 to anaphase for S74A and

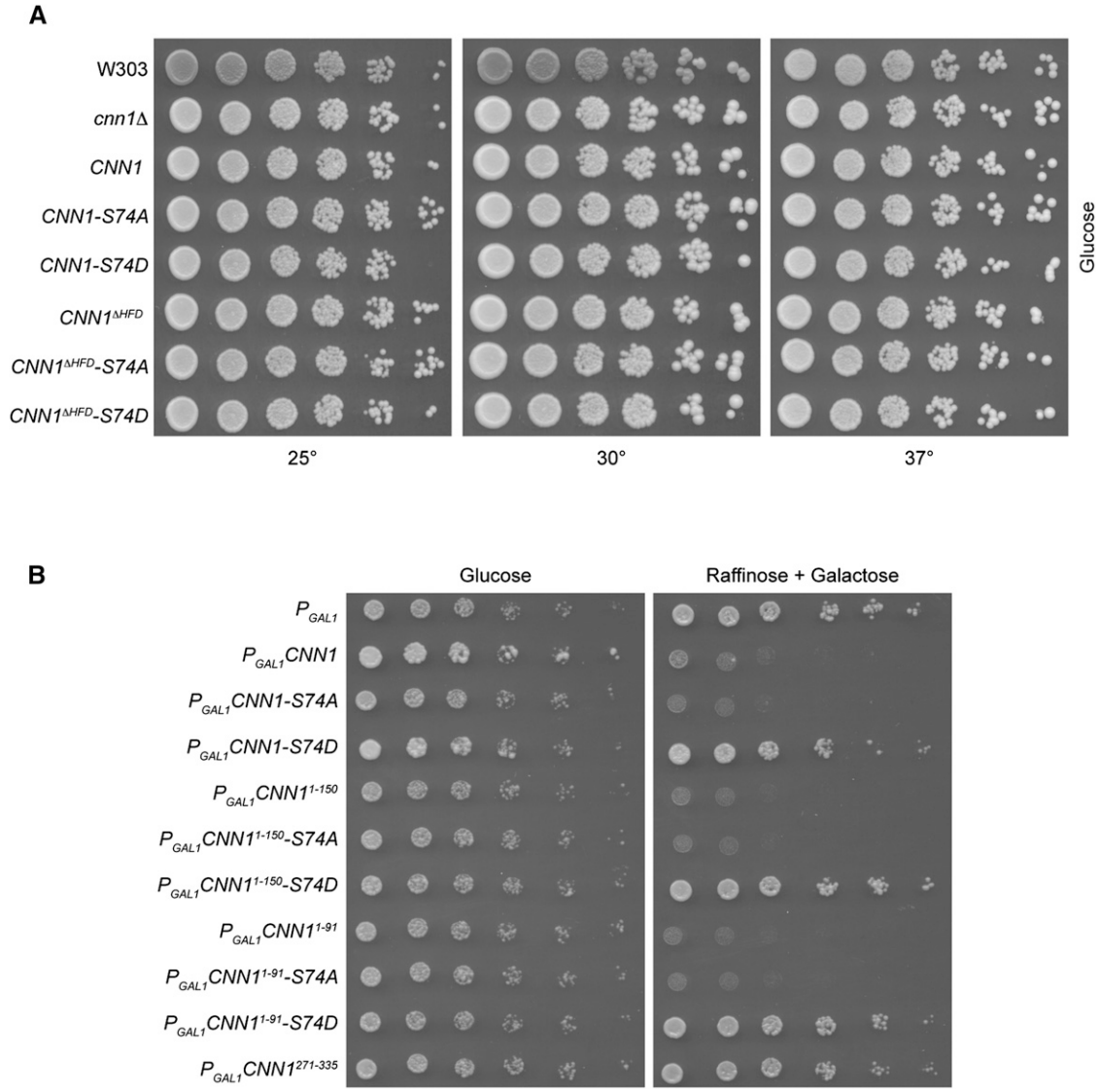

Figure 3 Functional significance of Cnn1 SIS and HFD. (A) Integration of *CNN1* and its mutants in a *cnn1Δ* strain. All the strains were serially diluted (1:5) on glucose plates and incubated at 25°, 30°, and 37°. (B) Serial dilution assay of strains overexpressing *CNN1* from *the* P_{GAL1} promoter. Left panel is repressed and right is inducing conditions. $Cnn1^{271–335}$, HFD.

appeared similar across all phases for S74D. Removing the HFD from Cnn1–GFP profoundly reduced the kinetochore recruitment level of $Cnn1^{\Delta HFD}$–GFP and S74A variant to 40–45% of interphase cells indicating the importance of the HFD but also demonstrating the ability of the SIS to mediate recruitment in pre-anaphase cells (Figure 6, A and B; Table S3). However, in anaphase, $Cnn1^{\Delta HFD}$–GFP and S74A variant were recruited similarly to Cnn1–GFP and increased signal intensities (only 12–16% cells had no signal), suggesting Cnn1 recruitment to anaphase kinetochores depends on the SIS–Ndc80 complex interaction. The S74A mutation does not result in increased signal intensities in preanaphase stages compared to wild type, indicating that S74A is not sufficient to mediate the increased recruitment of the SIS. However, when removing both the HFD- and SIS-mediated recruitment options, $Cnn1^{\Delta HFD}$–S74D–GFP did not localize detectably to kinetochores at any cell cycle stage (Figure 6, A and B). Hence, we demonstrate the *in vivo* disruption of the SIS–kinetochore contact by the S74D mutation. The expression levels of Cnn1–GFP and $Cnn1^{\Delta HFD}$–GFP were similar to those of their S74A and S74D variants, thus excluding differences in abundance or stability (Figure 6C). Notably, removing the HFD resulted in more diffused $Cnn1^{\Delta HFD}$–GFP signals at metaphase kinetochores (Figure S5). We also observed kinetochore localization of $Cnn1^{1–150}$–GFP via low-level P_{GAL} expression (2% raffinose) confirming that residues 151–361 are dispensable for the Cnn1 kinetochore localization (Figure S6). The use of the $Cnn1^{1–150}$–GFP indicates that additional regulatory post-translational sites or interaction motifs that aid in conferring cell cycle-specific localization and anaphase enrichment are within this N-terminal sequence. The fusion of the GFP epitope to different positions of Cnn1 (GFP positioned at the C terminus of Cnn1 after 150

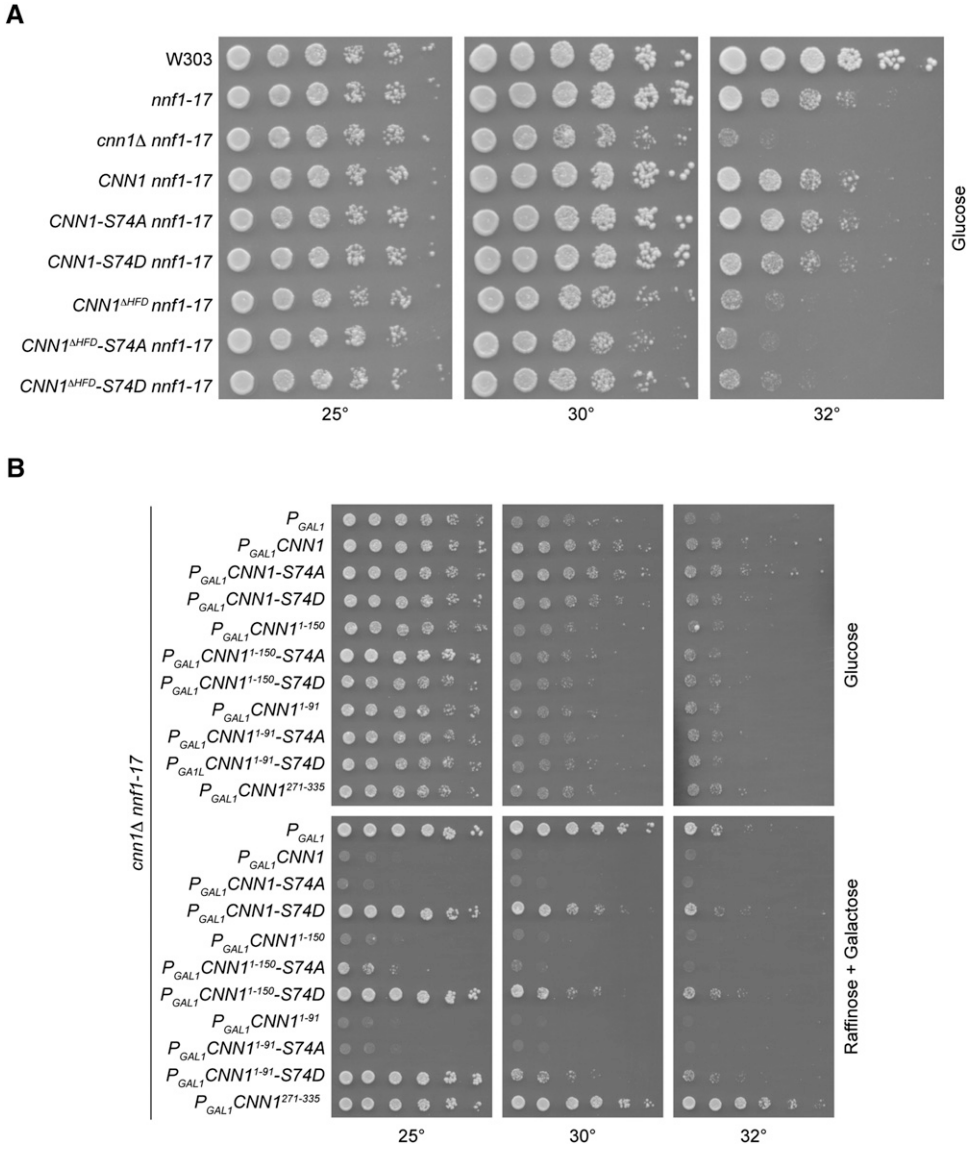

Figure 4 Genetic dissection of Cnn1 SIS and HFD activities. (A) Integration of *CNN1* and its mutants in the *cnn1Δ nnf1–17* strain incubated at 25° (permissive), 30° (semi-permissive), and 32° (nonpermissive). (B) Overexpression of *CNN1* and its phospho-null S74A versions results in a slow growth phenotype in the *cnn1Δ nnf1–17* background. The HFD (271–335) fully rescues (bottom). Cnn1 wild type and S74A (presence of HFD) weakly rescue at 32° due to incomplete P_{GAL} repression (top).

residues and after full-length Cnn1) suggests that the observed anaphase enrichment is not a result of a delay in fluorophore maturation as has recently been reported for some Cse4–GFP fusions (Wisniewski *et al.* 2014). In conclusion, the similar localization behaviors of ectopically expressed Cnn$^{1–150}$–GFP and single-integrant Cnn1$^{\Delta HFD}$–GFP indicate that both the HFD and SIS contribute to correct kinetochore localization of Cnn1 and only elimination of both prevents its localization.

Discussion

We demonstrate that Cnn1 forms preanaphase linkages at kinetochores and that linkages increase when Mps1 phosphorylation of S74 declines in anaphase. This pattern reflects the expression and activity of the Mps1 kinase, and its decrease in anaphase due to anaphase-promoting complex (APC)-mediated degradation (Palframan *et al.* 2006; Liu *et al.* 2011; Liu and Winey 2012). Cdc28 is another kinase known to target Cnn1 (Malvezzi *et al.* 2013), but its role remains unclear because the Cdc28 target residues in the N-terminal domain did not affect Cnn1–Spc24/Spc25 binding according to our yeast two-hybrid study (Table 1). Cnn1 was suggested to interact with the Ndc80 complex only at anaphase despite the presence of low co-IP signal in preanaphase (Schleiffer *et al.* 2012). Indeed, the preanaphase Ndc80 complex was shown to interact quantitatively with the Mtw1 complex via Dsn1–Spc24/Spc25 binding (Bock *et al.* 2012; Schleiffer *et al.* 2012). At anaphase entry, enriched and dephosphorylated Cnn1 outcompetes Dsn1 for Spc24/Spc25 binding (Bock *et al.* 2012; Schleiffer *et al.* 2012; Malvezzi *et al.* 2013). These studies suggested that the anaphase Cnn1–Ndc80 complex interaction promotes accurate and/or robust kinetochore–MT linkages (Bock *et al.* 2012; Schleiffer *et al.* 2012; Malvezzi *et al.* 2013). As explained below, our results indicate a previously unappreciated role for Cnn1 because we directly demonstrate, *in vivo*, the preanaphase interaction of Cnn1 with the kinetochore.

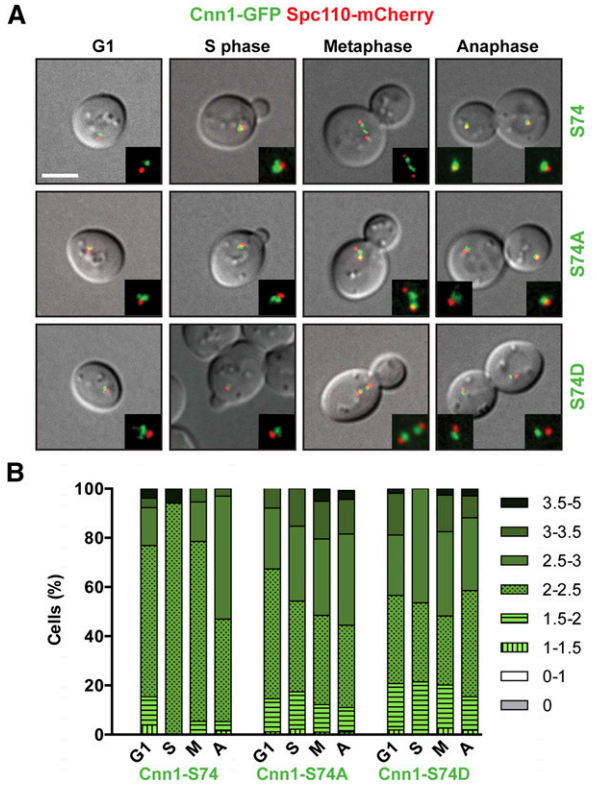

Figure 5 Localization of Cnn1 at the kinetochore. (A) Representative images of cells expressing Spc110–mCherry with Cnn1–GFP (top), Cnn1–S74A–GFP (middle), and Cnn1–S74D–GFP (bottom) in G1, S phase, metaphase, and anaphase. Bar, 5 μm. (B) Quantitation from A. Legend, increasing GFP:mCherry intensity ratio; gray, no GFP signal. $n \geq 231$ cells/strain.

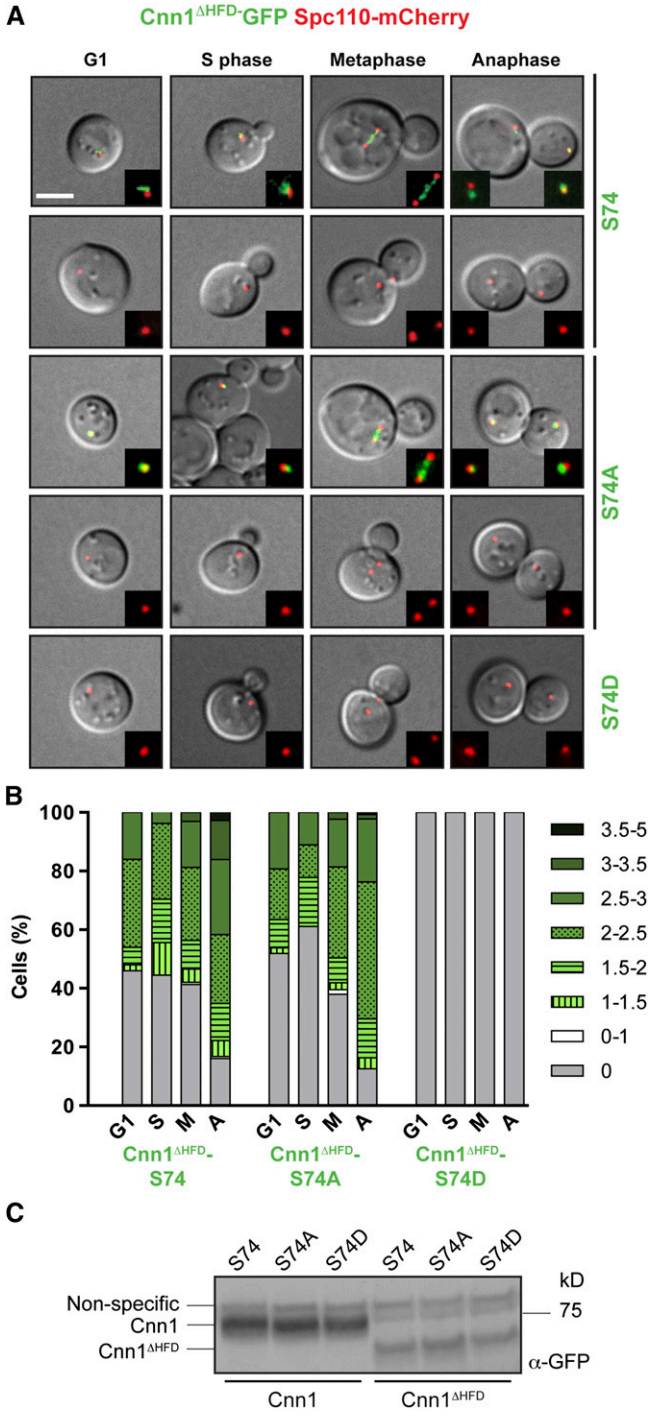

Figure 6 Dynamic localization of Cnn1$^{\Delta HFD}$ at the kinetochore. (A) Representative images of cells expressing Cnn1$^{\Delta HFD}$–GFP (top), Cnn1$^{\Delta HFD}$–S74A–GFP (middle), and Cnn1$^{\Delta HFD}$–S74D–GFP (bottom) in G1, S phase, metaphase, and anaphase. Bar, 5 μm. (B) Quantitation from A. (C) Western blot of Cnn1, Cnn1–S74A, Cnn1–S74D, Cnn1$^{\Delta HFD}$, Cnn1$^{\Delta HFD}$–S74A, and Cnn1$^{\Delta HFD}$–S74D probed with anti-GFP antibodies.

Involvement of the HFD in recruitment to the *CEN* is plausible, considering that CENP-T associates with *CEN* chromatin via its HFD (Nishino *et al.* 2012). The Cnn1–S74A and S74D in a full-length context altered localization profiles but did not eliminate *CEN* region recruitment compared to wild type, likely because the HFD is driving localization (Figure 5). We confirmed this because levels of HFD-lacking Cnn1 were reduced throughout the cell cycle (Figure 6). However, we identified a second kinetochore-localization activity in Cnn1: an N-terminal stretch of 66 residues that latches onto the Spc24/Spc25 interface. The dynamic recruitment of Cnn1 through the cell cycle depends on the HFD and SIS and the phosphorylation state of S74 because combining the S74D mutation and a lack of HFD completely eliminates the *CEN*/kinetochore signal (Figure 6). Our measurements demonstrate that part of the Cnn1 molecules at preanaphase kinetochores interact with the Ndc80 complexes because Cnn1 lacking its HFD is capable of recruitment via the SIS (Figure 6). Intriguingly, the S74A and wild-type SIS have similar localization behavior, suggesting another factor controls preanaphase SIS-mediated kinetochore localization in addition to the S74 dephosphorylation state. In addition, the recruitment patterns of full-length Cnn1–S74A and –S74D, while similar to wild type, had a greater proportion of signal prior to anaphase, indicating disrupted regulation of copy numbers. Further investigation is needed to identify the additional regulatory factor(s) that controls *CEN*/kinetochore recruitment of Cnn1 across the cell cycle.

From G1 till anaphase, the Ndc80 complex thus coexists in two bound states: the Mtw1 complex–Ndc80 complex interaction is constant through the cell cycle (Schleiffer *et al.* 2012) and the Cnn1–Ndc80 complex interaction occurs at preanaphase but increases at anaphase. Mps1 activity builds up from G1 through metaphase and hence was suggested to favor Mtw1 complex–Ndc80 complex binding, which may support a specific kinetochore conformation. We propose that Mps1 may only restrain Cnn1 at metaphase because Mps1 expression levels are low in G1 (Palframan *et al.* 2006) and Cnn1 is mostly dephosphorylated in G1 (Bock *et al.* 2012; Schleiffer *et al.* 2012), whereas Cdc28 appears to control Cnn1 phosphorylation at S phase (Malvezzi *et al.* 2013) (Figure 7A). In addition, other factors may limit the Cnn1–Ndc80 interaction.

Binding of the Ndc80 complex to Cnn1 tethers the complex to the *CEN*. However, this tethering does not serve to recruit the Ndc80 complex during kinetochore assembly as cells lacking Cnn1 do not suffer from reduced levels of the Ndc80 complex, nor a reduction in the Mtw1 and Spc105 complexes (Bock *et al.* 2012). In contrast, mammalian CENP-T actively recruits the Ndc80 complex to *CEN*s (Gascoigne *et al.* 2011) and the middle region of CENP-T appears to be flexible and assists in kinetochore stretching when it undergoes tension (Perpelescu and Fukagawa 2011; Suzuki *et al.* 2011; Westhorpe and Straight 2013). Similarly, the preanaphase Cnn1 linkages may allow a proper intrakinetochore stretch required for chromosome biorientation, as shown for CENP-T (Suzuki *et al.* 2014). Next to altering the interactions between the KMN complexes, the preanaphase Cnn1 linkages may be involved in tension sensing during sister–kinetochore attachment and biorientation, which are also regulated by Mps1 (Weiss and Winey 1996). In addition, other kinases regulate Cnn1, including Cdc28-dependent multisite phosphorylation, leading to a maximal Cnn1 phosphorylation reached at metaphase (Figure 7B). The metaphase phosphorylation peak is followed by rapid dephosphorylation resulting in Cnn1 enrichment to kinetochores at anaphase onset (Bock *et al.* 2012). A Cdc28-dependent threshold triggers the Skp1–Cul1–F box (SCF)-mediated destruction of Sic1 at S phase entry (Koivomagi *et al.* 2011, 2013) and the Cnn1 metaphase phospho threshold may initiate phosphatase activity on S74 and surrounding residues. S74 from Cnn1 likely needs surrounding sites to be phosphorylated because the $Cnn1^{60–84}$ sequence can replace a similar Ndc80 binding motif in the Dsn1 protein, indicating S74 is not phosphorylated in that context (Malvezzi *et al.* 2013). In addition, the phosphorylation sites contributing to the phospho threshold must be within the N-terminal residues because we show that the $Cnn^{1–150}$–GFP construct behaved similarly to full-length Cnn1 (Figure S5).

We note that S74 is conserved among most budding yeasts, except for *C. glabrata*, which has an aspartic acid (D63) at this site demonstrating an evolutionary difference in phosphorylation sites. This change in phospho regulation could be an important feature in understanding the evolution of phosphorylation sites and is consistent with positional flexibility of Cdk1

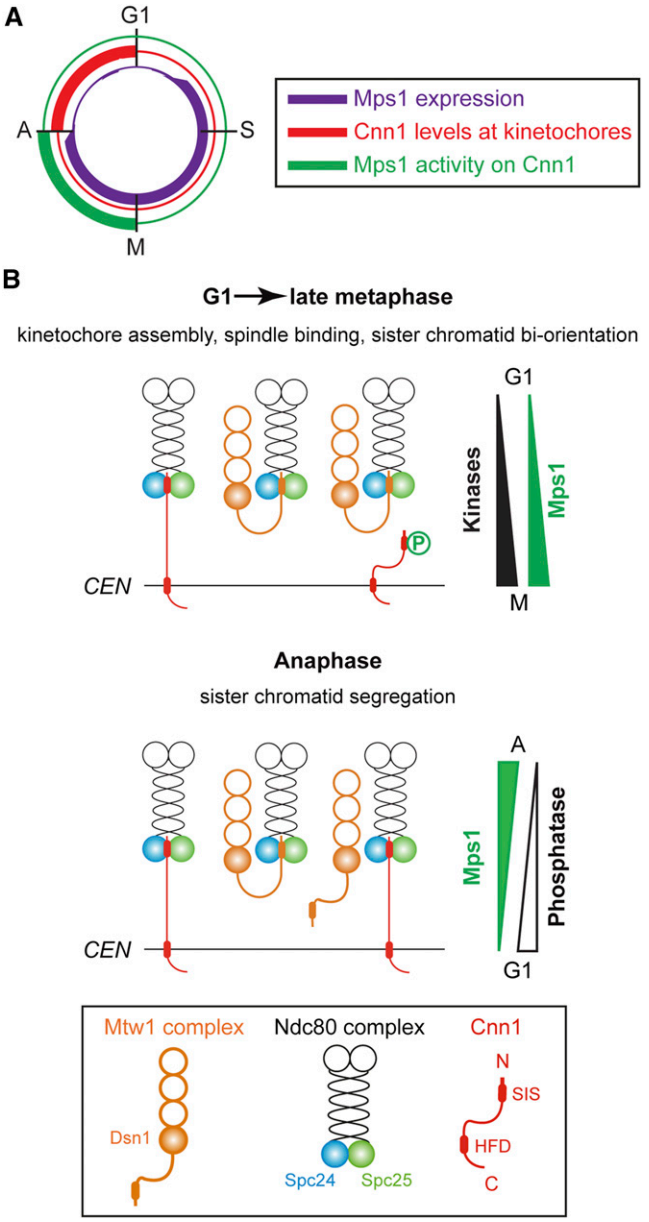

Figure 7 Role of SIS and HFD in chromosome segregation. (A) Schematic depicting the expression and activity of Mps1 relative to Cnn1 through the cell cycle. (B) Model delineating the regulation of Cnn1 by Mps1, additional kinases, and phosphatases.

sites among orthologous proteins (Holt *et al.* 2009). The transition from negative regulation of the Cnn1–Ndc80 interaction by Mps1 to the suggested positive regulation by CDK1 in the vertebrate orthologs (Nishino *et al.* 2013) is a striking example of regulatory transition involving kinases through evolution.

Next to driving Cnn1 to kinetochores, the HFD may have additional roles. The association of the Cnn1 HFD can change the environment and activity of the *CEN* region and/or the kinetochore, as overexpressing the HFD in a kinetochore-defective strain rescued its viability (Figure 4B). The *nnf1–17* strain has reduced levels of the Mtw1 and Ndc80 complexes (De Wulf *et al.* 2003; Westermann *et al.* 2003), resulting in an

unstable kinetochore; hence, we hypothesize that Cnn1 HFD promotes kinetochore function possibly by incorporation into chromatin. This is consistent with the more diffuse signal observed for Cnn1$^{\Delta HFD}$–GFP (Figure S5) compared to Cnn1–GFP. Although the *CEN*–HFD interaction has not been delineated in yeast, Cnn1 may form a nucleosome-like structure as suggested for CENP-T (Nishino *et al.* 2012; Nishino *et al.* 2013; Takeuchi *et al.* 2014). However, Basilico *et al.* (2014) proposed a nonnucleosomal population, first because the CENP–HIKM complex is required for CENP-T recruitment and second because CENP-T turns over at *CEN*s (Prendergast *et al.* 2011). Similarly, the abrupt SIS-mediated enrichment of Cnn1 in anaphase suggests a nonnucleosomal population and prompts further studies examining exchange mechanisms for Cnn1 and other centromere-associated proteins.

Acknowledgments

We thank Sara Barozzi for assisting with microscopy and Sebastiano Pasqualato for the Cnn1–Spc24/Spc25 structure manipulations. The His6–Spc24/Spc25 plasmid was kindly provided by Stefan Westermann (Research Institute of Molecular Pathology, Vienna). K.S.T. was supported by a Special Incentive Research Grant (SIRG) award administered through the Purdue University Center for Cancer Research (PUCCR) and by a Purdue Research Foundation fellowship. Support for this publication was possible by funding from National Institute of General Medical Sciences R01GM087461 (T.R.H.), P30 CA023168 (PUCCR), and investigator grant 8840 from the Italian Association for Cancer Research (P.D.W.). K.S.T. performed fluorescence imaging using the Nikon A1 system, *in vitro* binding, yeast two-hybrid, and genetic experiments. P.D.W., C.P., and A.O. performed quantitative fluorescence imaging using the DeltaVision system. K.S.T., P.D.W., and T.R.H. interpreted experimental data and wrote the manuscript. Experiments were conceived by P.D.W. and T.R.H. The authors declare no competing financial interests.

Literature Cited

Alushin, G. M., V. H. Ramey, S. Pasqualato, D. A. Ball, N. Grigorieff *et al.*, 2010 The Ndc80 kinetochore complex forms oligomeric arrays along microtubules. Nature 467: 805–810.

Basilico, F., S. Maffini, J. R. Weir, D. Prumbaum, A. M. Rojas *et al.*, 2014 The pseudo GTPase CENP-M drives human kinetochore assembly. eLife 3: e02978.

Bock, L. J., C. Pagliuca, N. Kobayashi, R. A. Grove, Y. Oku *et al.*, 2012 Cnn1 inhibits the interactions between the KMN complexes of the yeast kinetochore. Nat. Cell Biol. 14: 614–624.

Breitkreutz, A., H. Choi, J. R. Sharom, L. Boucher, V. Neduva *et al.*, 2010 A global protein kinase and phosphatase interaction network in yeast. Science 328: 1043–1046.

Cheeseman, I. M., 2014 The kinetochore. Cold Spring Harb. Perspect. Biol. 6: a015826.

Cheeseman, I. M., J. S. Chappie, E. M. Wilson-Kubalek, and A. Desai, 2006 The conserved KMN network constitutes the core microtubule-binding site of the kinetochore. Cell 127: 983–997.

Cheeseman, L. M., S. Anderson, M. Jwa, E. M. Green, J. S. Kang *et al.*, 2002 Phospho-regulation of kinetochore-microtubule attachments by the aurora kinase Ipl1p. Cell 111: 163–172.

Ciferri, C., S. Pasqualato, E. Screpanti, G. Varetti, S. Santaguida *et al.*, 2008 Implications for kinetochore-microtubule attachment from the structure of an engineered Ndc80 complex. Cell 133: 427–439.

De Wulf, P., A. D. McAinsh, and P. K. Sorger, 2003 Hierarchical assembly of the budding yeast kinetochore from multiple subcomplexes. Genes Dev. 17: 2902–2921.

De Wulf, P., F. Montani, and R. Visintin, 2009 Protein phosphatases take the mitotic stage. Curr. Opin. Cell Biol. 21: 806–815.

Edgar, R. C., 2004 MUSCLE: multiple sequence alignment with high accuracy and high throughput. Nucleic Acids Res. 32: 1792–1797.

Eswar, N., B. Webb, M. A. Marti-Renom, M. S. Madhusudhan, D. Eramian *et al.*, 2006 Comparative protein structure modeling using Modeller. Curr. Protoc. Bioinformatics Chapter 5, Unit 5.6.

Gascoigne, K. E., K. Takeuchi, A. Suzuki, T. Hori, T. Fukagawa *et al.*, 2011 Induced ectopic kinetochore assembly bypasses the requirement for CENP-A nucleosomes. Cell 145: 410–422.

Hansson, M. D., K. Rzeznicka, M. Rosenback, M. Hansson, and N. Sirijovski, 2008 PCR-mediated deletion of plasmid DNA. Anal. Biochem. 375: 373–375.

Holt, L. J., B. B. Tuch, J. Villen, A. D. Johnson, S. P. Gygi *et al.*, 2009 Global analysis of Cdk1 substrate phosphorylation sites provides insights into evolution. Science 325: 1682–1686.

Hori, T., M. Amano, A. Suzuki, C. B. Backer, J. P. Welburn *et al.*, 2008 CCAN makes multiple contacts with centromeric DNA to provide distinct pathways to the outer kinetochore. Cell 135: 1039–1052.

James, P., J. Halladay, and E. A. Craig, 1996 Genomic libraries and a host strain designed for highly efficient two-hybrid selection in yeast. Genetics 144: 1425–1436.

Koivomagi, M., M. Ord, A. Iofik, E. Valk, R. Venta *et al.*, 2013 Multisite phosphorylation networks as signal processors for Cdk1. Nat. Struct. Mol. Biol. 20: 1415–1424.

Koivomagi, M., E. Valk, R. Venta, A. Iofik, M. Lepiku *et al.*, 2011 Cascades of multisite phosphorylation control Sic1 destruction at the onset of S phase. Nature 480: 128–131.

Liu, C., D. van Dyk, V. Choe, J. Yan, S. Majumder *et al.*, 2011 Ubiquitin ligase Ufd2 is required for efficient degradation of Mps1 kinase. J. Biol. Chem. 286: 43660–43667.

Liu, X., and M. Winey, 2012 The MPS1 family of protein kinases. Annu. Rev. Biochem. 81: 561–585.

Malvezzi, F., and S. Westermann, 2014 "Uno, nessuno e centomila": the different faces of the budding yeast kinetochore. Chromosoma 123: 447–457.

Malvezzi, F., G. Litos, A. Schleiffer, A. Heuck, K. Mechtler *et al.*, 2013 A structural basis for kinetochore recruitment of the Ndc80 complex via two distinct centromere receptors. EMBO J. 32: 409–423.

Nishino, T., K. Takeuchi, K. E. Gascoigne, A. Suzuki, T. Hori *et al.*, 2012 CENP-T-W-S-X forms a unique centromeric chromatin structure with a histone-like fold. Cell 148: 487–501.

Nishino, T., F. Rago, T. Hori, K. Tomii, I. M. Cheeseman *et al.*, 2013 CENP-T provides a structural platform for outer kinetochore assembly. EMBO J. 32: 424–436.

Palframan, W. J., J. B. Meehl, S. L. Jaspersen, M. Winey, and A. W. Murray, 2006 Anaphase inactivation of the spindle checkpoint. Science 313: 680–684.

Perpelescu, M., and T. Fukagawa, 2011 The ABCs of CENPs. Chromosoma 120: 425–446.

Prendergast, L., C. van Vuuren, A. Kaczmarczyk, V. Doering, D. Hellwig *et al.*, 2011 Premitotic assembly of human CENPs -T and -W switches centromeric chromatin to a mitotic state. PLoS Biol. 9: e1001082.

Schleiffer, A., M. Maier, G. Litos, F. Lampert, P. Hornung *et al.*, 2012 CENP-T proteins are conserved centromere receptors of the Ndc80 complex. Nat. Cell Biol. 14: 604–613.

Sikorski, R. S., and P. Hieter, 1989 A system of shuttle vectors and yeast host strains designed for efficient manipulation of DNA in *Saccharomyces cerevisiae*. Genetics 122: 19–27.

Suzuki, A., T. Hori, T. Nishino, J. Usukura, A. Miyagi *et al.*, 2011 Spindle microtubules generate tension-dependent changes in the distribution of inner kinetochore proteins. J. Cell Biol. 193: 125–140.

Suzuki, A., B. L. Badger, X. Wan, J. G. DeLuca, and E. D. Salmon, 2014 The architecture of CCAN proteins creates a structural integrity to resist spindle forces and achieve proper intrakinetochore stretch. Dev. Cell 30: 717–730.

Takeuchi, K., T. Nishino, K. Mayanagi, N. Horikoshi, A. Osakabe *et al.*, 2014 The centromeric nucleosome-like CENP-T-W-S-X complex induces positive supercoils into DNA. Nucleic Acids Res. 42: 1644–1655.

Thompson, J. D., T. J. Gibson, F. Plewniak, F. Jeanmougin, and D. G. Higgins, 1997 The CLUSTAL_X windows interface: flexible strategies for multiple sequence alignment aided by quality analysis tools. Nucleic Acids Res. 25: 4876–4882.

Wei, R. R., J. Al-Bassam, and S. C. Harrison, 2007 The Ndc80/HEC1 complex is a contact point for kinetochore-microtubule attachment. Nat. Struct. Mol. Biol. 14: 54–59.

Weiss, E., and M. Winey, 1996 The *Saccharomyces cerevisiae* spindle pole body duplication gene MPS1 is part of a mitotic checkpoint. J. Cell Biol. 132: 111–123.

Westermann, S., I. M. Cheeseman, S. Anderson, J. R. Yates, D. G. Drubin *et al.*, 2003 Architecture of the budding yeast kinetochore reveals a conserved molecular core. J. Cell Biol. 163: 215–222.

Westermann, S., D. G. Drubin, and G. Barnes, 2007 Structures and functions of yeast kinetochore complexes. Annu. Rev. Biochem. 76: 563–591.

Westhorpe, F. G., and A. F. Straight, 2013 Functions of the centromere and kinetochore in chromosome segregation. Curr. Opin. Cell Biol. 25: 334–340.

Wisniewski, J., B. Hajj, J. Chen, G. Mizuguchi, H. Xiao *et al.*, 2014 Imaging the fate of histone Cse4 reveals de novo replacement in S phase and subsequent stable residence at centromeres. eLife 3: e02203.

Wong, J., Y. Nakajima, S. Westermann, C. Shang, J. S. Kang *et al.*, 2007 A protein interaction map of the mitotic spindle. Mol. Biol. Cell 18: 3800–3809.

Communicating editor: N. Hollingsworth

GENETICS

Supporting Information
http://www.genetics.org/lookup/suppl/doi:10.1534/genetics.115.175786/-/DC1

The Mps1 Kinase Modulates the Recruitment and Activity of Cnn1^{CENP-T} at *Saccharomyces cerevisiae* Kinetochores

Kriti Shrestha Thapa, Amanda Oldani, Cinzia Pagliuca, Peter De Wulf, and Tony R. Hazbun

DOI: 10.1534/genetics.115.175786

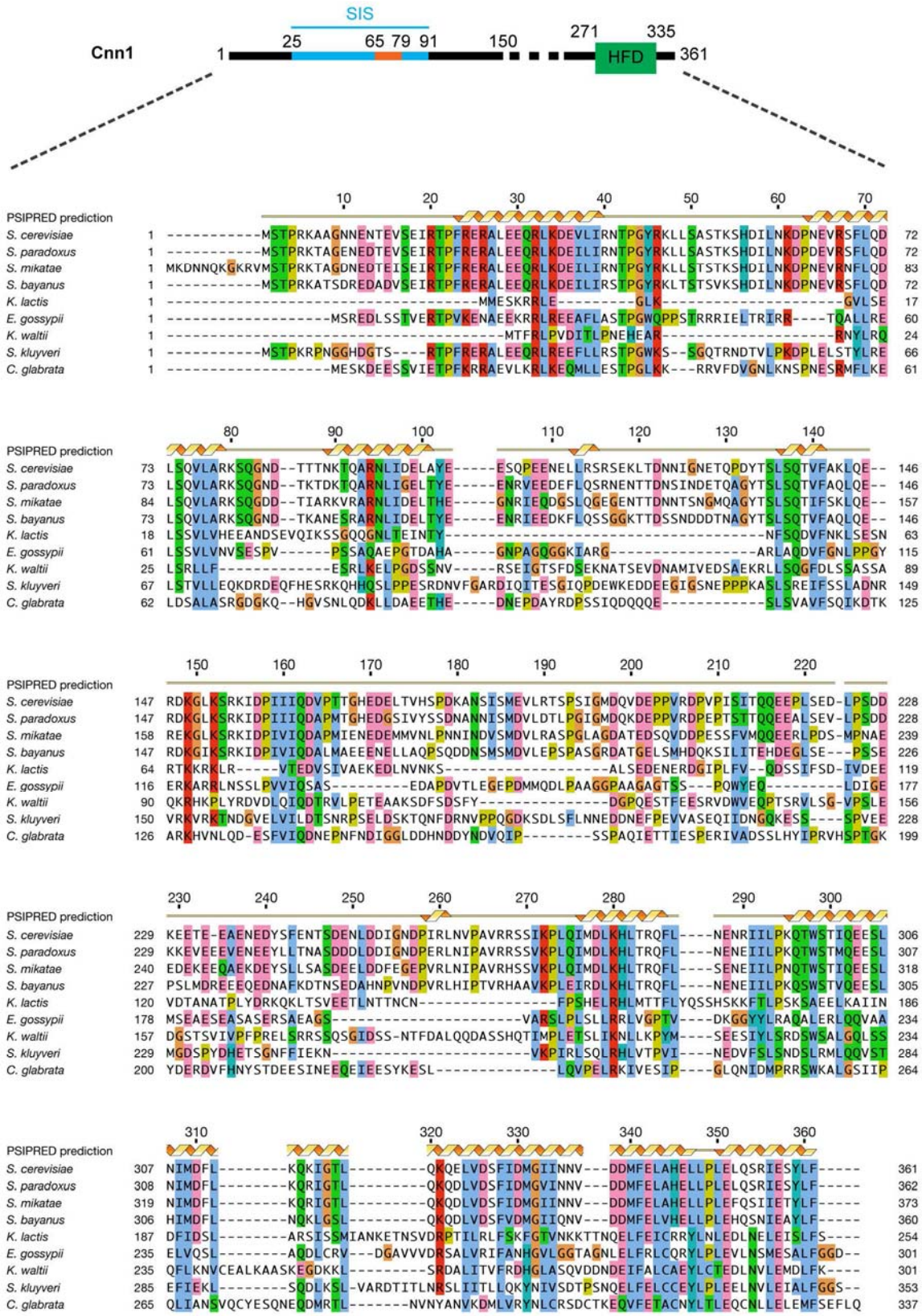

Figure S1 Cnn1 multiple sequence alignment with other fungal species depicting the alignment for the full length proteins.

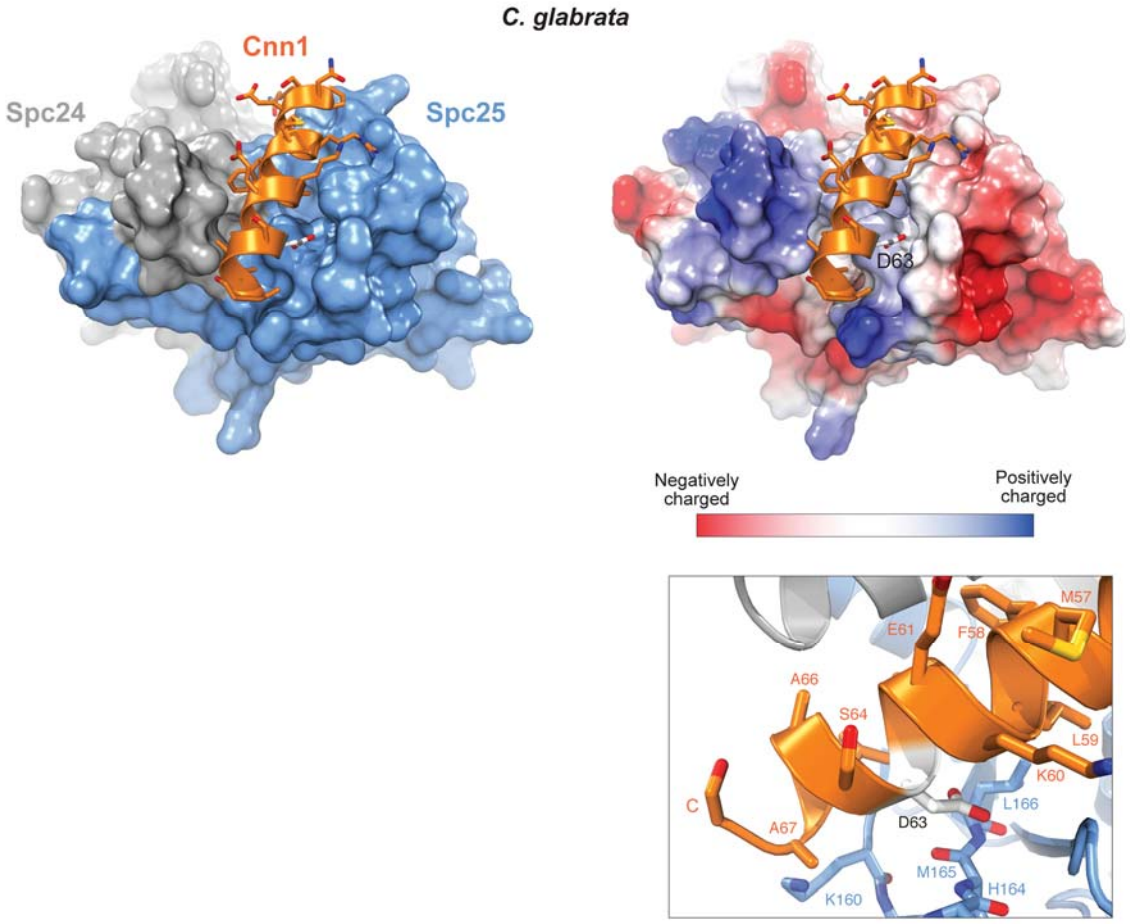

Figure S2 Crystal structure of *C. glabrata* Cnn1$^{60\text{-}84}$ in complex with Spc24/25. View of Cnn1-D63 positioned within a pocket formed by Spc25 residues (top right). Cnn1-D63 projects into a positively charged environment (bottom right) compared to the *S. cerevisiae* residue at the same position in the helix, S74, which projects into a negatively charged environment that would prevent an interaction if S74 is phosphorylated.

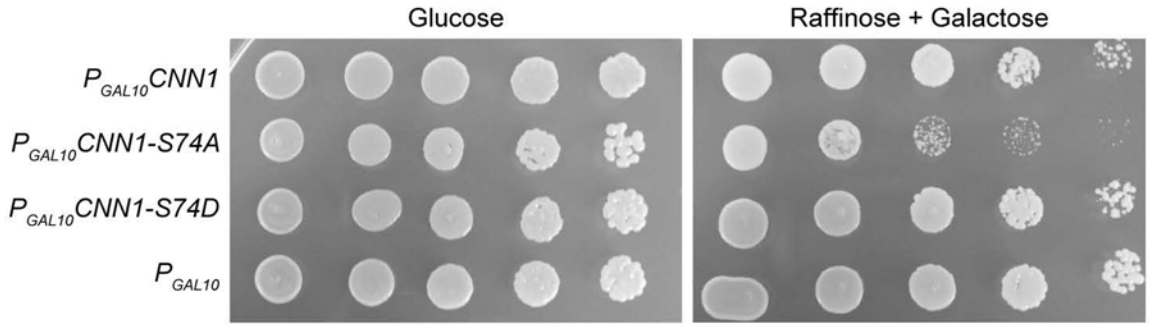

Figure S3 Overexpression of *CNN1*, *CNN1-S74A* and *CNN1-S74D* from P_{GAL10} promoter in W303. All the strains were serially diluted on 2% glucose plate (left) and 2% raffinose and 2% galactose plate (right). Note *CNN1-S74A* has decreased viability compared to *CNN1* under the P_{GAL10} promoter background.

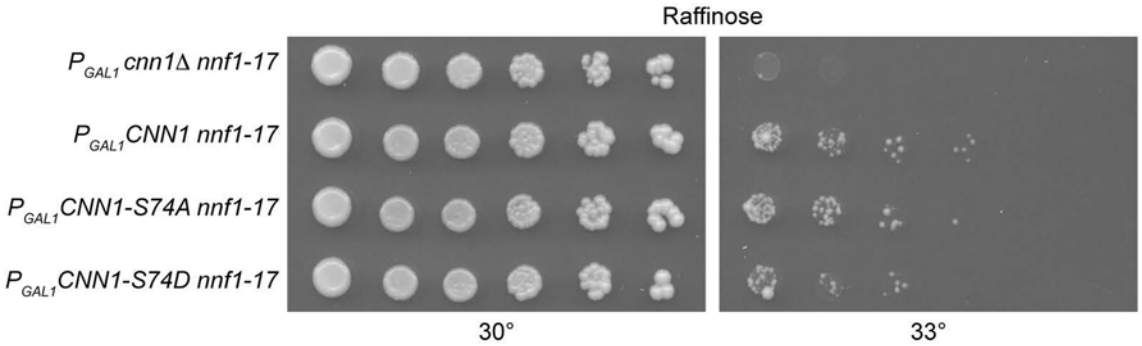

Figure S4 Overexpression of *CNN1*, *CNN1-S74A* and *CNN1-S74D* in *cnn1Δ nnf1-17* strain. All the strains were serially diluted on a 2% raffinose only plate (low expression levels) and incubated at 30° (semi-permissive) and 33° (non-permissive) for 5 d. Note *CNN1* and *CNN1-S74A* (in presence of HFD) generate stronger rescue that the *CNN1-S74D* mutant.

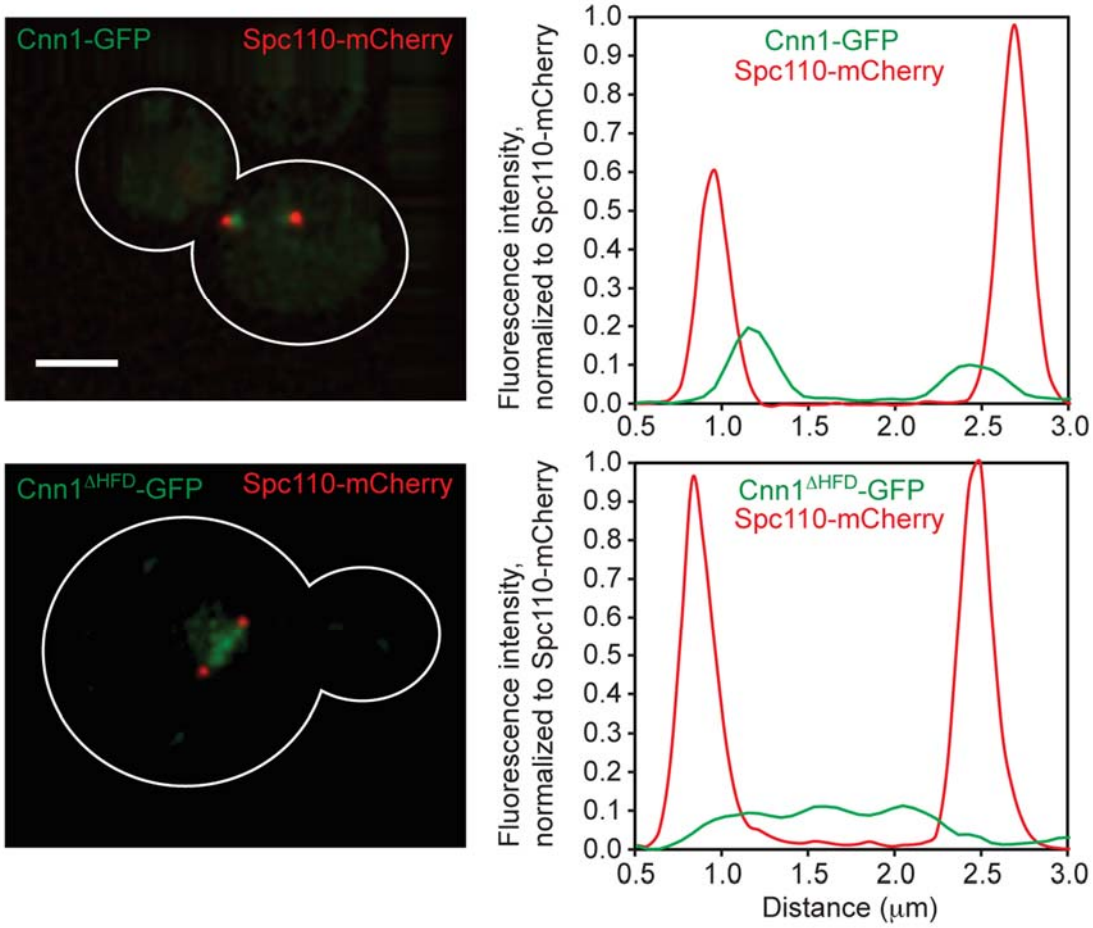

Figure S5 Representative images of a close-up view of Cnn1-GFP Spc110-mCherry and Cnn1$^{\Delta HFD}$-GFP Spc110-mCherry cells at metaphase (left). The fluorescence intensity is normalized and plotted along the cell axis (right). Bar = 2 μm

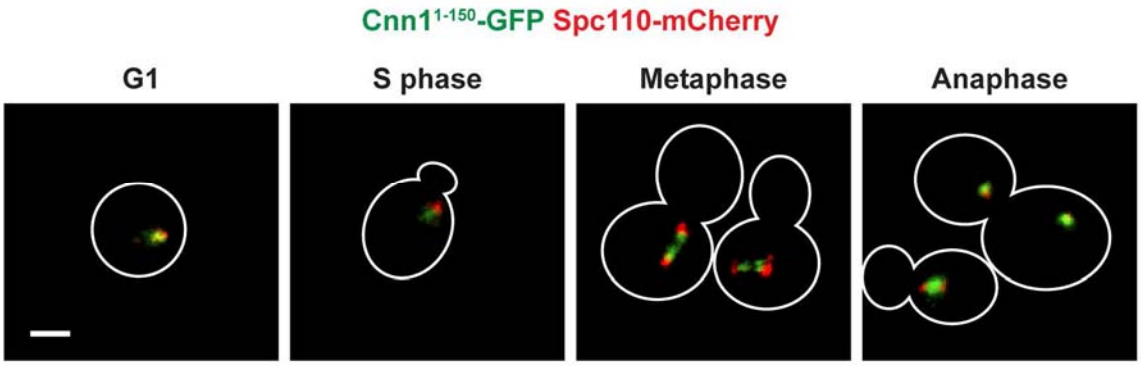

Figure S6 Representative images of *SPC110-mCherry* cells overexpressing *Cnn1$^{1-150}$-GFP* from P_{GAL} promoter in G1, S phase, metaphase and anaphase. Cells were induced with 2% raffinose before the images were captured. Bar = 2 μm.

Table S1 Yeast strains used in this study

Strain	Other Name	Genotype	Source
THY2114	PDW001 (W303)	*leu2-3,112 trp1-1 can1-100 ura3-1 ade2-1 his3-11,15*	Nasmyth Lab
KTY2248		*pESC URA3 P_{GAL1}-myc*	This study
KTY2249		*pESC URA3 P_{GAL1}-CNN1-myc*	This study
KTY2250		*pESC URA3 P_{GAL1}-CNN1-S74A-myc*	This study
KTY2251		*pESC URA3 P_{GAL1}-CNN1-S74D-myc*	This study
KTY2252		*pESC URA3 P_{GAL1}-CNN1(1-150)-myc*	This study
KTY2253		*pESC URA3 P_{GAL1}-CNN1(1-150)-S74A-myc*	This study
KTY2254		*pESC URA3 P_{GAL1}-CNN1(1-150)-S74D-myc*	This study
KTY2255		*pESC URA3 P_{GAL1}-CNN1(1-91)-myc*	This study
KTY2256		*pESC URA3 P_{GAL1}-CNN1(1-91)-S74A-myc*	This study
KTY2257		*pESC URA3 P_{GAL1}-CNN1(1-91)-S74D-myc*	This study
KTY2258		*pESC URA3 P_{GAL1}-CNN1(271-335)-myc*	This study
THY2107	PDW112 (GEY138)	*MATα nnf1-17::LEU2*	Euskirchen Lab
THY2115	PDW1422	*cnn1Δ::kanMX4, nnf1-17::LEU2*	De Wulf Lab
KTY2208		*THY2115 pRS306-CNN1-GFP*	This study
KTY2209		*THY2115 pRS306-CNN1-S74A-GFP*	This study
KTY2210		*THY2115 pRS306-CNN1-S74D-GFP*	This study
KTY2307		*THY2115 pRS306-CNN1(Δ271-335)-GFP*	This study
KTY2308		*THY2115 pRS306-CNN1(Δ271-335)-S74A-GFP*	This study
KTY2309		*THY2115 pRS306-CNN1(Δ271-335)-S74D-GFP*	This study
KTY2260		*THY2115 pESC URA3 P_{GAL1}-myc*	This study
KTY2261		*THY2115 pESC URA3 P_{GAL1}-CNN1-myc*	This study
KTY2262		*THY2115 pESC URA3 P_{GAL1}-CNN1-S74A-myc*	This study
KTY2263		*THY2115 pESC URA3 P_{GAL1}-CNN1-S74D-myc*	This study
KTY2264		*THY2115 pESC URA3 P_{GAL1}-cnn1(1-150)-myc*	This study
KTY2265		*THY2115 pESC URA3 P_{GAL1}-cnn1(1-150)-S74A-myc*	This study
KTY2266		*THY2115 pESC URA3 P_{GAL1}-cnn1(1-150)-S74D-myc*	This study
KTY2267		*THY2115 pESC URA3 P_{GAL1}-cnn1(1-91)-myc*	This study
KTY2268		*THY2115 pESC URA3 P_{GAL1}-cnn1(1-91)-S74A-myc*	This study
KTY2269		*THY2115 pESC URA3 P_{GAL1}-cnn1(1-91)-S74D-myc*	This study
KTY2270		*THY2115 pESC URA3 P_{GAL1}-CNN1(271-335)-myc*	This study
THY2110	PDW2216	*cnn1Δ::natMX4, SPC110-mCherry::hphMX3*	De Wulf Lab
KTY2147		*THY2110 pRS306-CNN1-GFP*	This study
KTY2149		*THY2110 pRS306-CNN1-S74D-GFP*	This study
KTY2158		*THY2110 pRS306-CNN1(Δ271-335)-GFP*	This study

KTY2160		*THY2110 pRS306-CNN1(Δ271-335)-S74D-GFP*	This study
KTY2241		*pESC URA3 P_{GAL10}-FLAG*	This study
KTY2242		*pESC URA3 P_{GAL10}-CNN1-FLAG*	This study
KTY2243		*pESC URA3 P_{GAL10}-CNN1-S74A-FLAG*	This study
KTY2244		*pESC URA3 P_{GAL10}-CNN1-S74D-FLAG*	This study
KTY2146		*THY2110 pAG414 P_{GAL1}-CNN1(1-150)-GAL4-DBD(1-74)-EGFP*	This study
THY2468	PJ69-4a	*MATa trp1-901 leu2-3,112 ura3-52 his3-200 gal4 gal80 LYS2:: P_{GAL1}-HIS3 P_{GAL2}-ADE2 met2:: P_{GAL7}-lacZ*	Lab Collection
THY2469	PJ69-4α	*MATα trp1-901 leu2-3,112 ura3-52 his3-200 gal4 gal80 LYS2:: P_{GAL1}-HIS3 P_{GAL2}2-ADE2 met2:: P_{GAL7}-lac*	Lab Collection

Table S2 Plasmids used in this study

Plasmid	Relevant markers	Source
PKT0226	*CNN1(25-47)* in pGEX-6P-1 (GST)	This study
PKT0227	*CNN1(25-60*)in pGEX-6P-1 (GST)	This study
PKT0228	*CNN1(25-91)* in pGEX-6P-1 (GST)	This study
PKT0229	*CNN1(47-60)* in pGEX-6P-1 (GST)	This study
PTH1917	pGEX-4T-2 (GST)	Hazbun Lab
PKT0211	*CNN1(1-150)* in pGEX-6P-1 (GST)	Hazbun Lab
PKT0230	*CNN1(47-91)* in pGEX-6P-1 (GST)	This study
PKT0231	*CNN1(60-91)* in pGEX-6P-1 (GST)	This study
PKT0232	*CNN1(91-150)* in pGEX-6P-1 (GST)	This study
PKT0213	*DJ1-E16D* in pGEX-6P-1 (GST)	This study
PSW0119	*SPC24/25* in pETDuett (His6)-coexpressed	Westermann Lab
PKT0106	*CNN1(1-150)* in pET28b (His6)	This study
PKT0107	*CNN1(1-150)-S74A* in pET28b (His6)	This study
PKT0108	*CNN1(1-150)-S74D* in pET28b (His6)	This study
PKT0101	*SPC24* in pGEX-6P-1 (GST)	Hazbun Lab
PKT0103	*SPC25(128-222)* in pGEX-6P-1 (GST)	Hazbun Lab
PKT0212	*CNN1(1-150)-S74A* in pGEX-6P-1 (GST)	This study
PKT0210	*CNN1(1-150)-T91D* in pET28b (His6)	This study
pOBD2-Nuf2	*NUF2* in pOBD2 (Gal4 DNA-binding domain)	Hazbun Lab
pOBD2-Spc24	*SPC24* in pOBD2 (Gal4 DNA-binding domain)	Hazbun Lab
pOBD2-Spc25	*SPC25* in pOBD2 (Gal4 DNA-binding domain)	Hazbun Lab
PKT0113	*CNN1* in pOAD (Gal4 activation domain)	Hazbun Lab
PRG1955	*CNN1 (1-150)-T14A, S17A, T21A, S74A* in pOAD (Gal4 activation domain)	This study
PRG1956	*CNN1(1-150)-T14D, S17D, T21D, S74D* in pOAD (Gal4 activation domain)	This study
PKT0116	*CNN1-S177A* in pOAD (Gal4 activation domain)	This study
PKT0117	*CNN1-S177D* in pOAD (Gal4 activation domain)	This study
PKT0114	*CNN1-S74A* in pOAD (Gal4 activation domain)	This study
PKT0115	*CNN1-S74D* in pOAD (Gal4 activation domain)	This study
PKT0207	*CNN1(1-150)* in pOAD (Gal4 activation domain)	Hazbun Lab
PKT0109	*CNN1(1-150)-S74A* in pOAD (Gal4 activation domain)	This study
PKT0110	*CNN1(1-150)-S74D* in pOAD (Gal4 activation domain)	This study
PKT0111	*CNN1(1-150)-17A* in pOAD (Gal4 activation domain)	This study
PKT0112	*CNN1(1-150)-17D* in pOAD (Gal4 activation domain)	This study
PKT0205	*CNN1(1-150)-T53D* in pOAD (Gal4 activation domain)	This study
PKT0208	*CNN1(1-150)-T86D* in pOAD (Gal4 activation domain)	This study
PRG1948	*CNN1-S268A, S269A* in pOAD (Gal4 activation domain)	This study
PRG1949	*CNN1-S268D, S269D* in pOAD (Gal4 activation domain)	This study
PKT0201	*CNN1(1-150)-T3A* in pOAD (Gal4 activation domain)	This study
PKT0202	*CNN1(1-150)-T3D* in pOAD (Gal4 activation domain)	This study
PKT0203	*CNN1(1-150)-T21A* in pOAD (Gal4 activation domain)	This study
PKT0204	*CNN1(1-150)-T21D* in pOAD (Gal4 activation domain)	This study
PRG1950	*CNN1(1-150)-T42A, S81A, T121A* in pOAD (Gal4 activation domain)	This study
PKT0146	*pESC URA3*	Hazbun lab
PKT0139	P_{CNN1}*-CNN1-GFP* in pRS306 (integrating)	This study
PKT0141	P_{CNN1}*-CNN1-S74A-GFP* in pRS306 (integrating)	This study
PKT0142	P_{CNN1}*-CNN1-S74D-GFP* in pRS306 (integrating)	This study
PKT0143	P_{CNN1}*-CNN1(Δ271-335)-GFP* in pRS306 (integrating)	This study
PKT0144	P_{CNN1}*-CNN1(Δ271-335)-S74A-GFP* in pRS306 (integrating)	This study
PKT0145	P_{CNN1}*-CNN1(Δ271-335)-S74D-GFP* in pRS306 (integrating)	This study

Table S3 Localization data from Cnn1-GFP expressing strains represented in Figures 5 and 6

Strain	Phase	Intensity Ratio[a]								n[b]
		0	0-1	1-1.5	1.5-2	2-2.5	2.5-3	3-3.5	3.5-5	
Cnn1-GFP	G1	0.00	0.00	3.85	11.54	61.54	15.38	3.85	3.85	26
	S	0.00	0.00	0.00	0.00	94.12	0.00	0.00	5.88	17
	M	0.00	0.00	0.00	5.36	73.21	16.07	5.36	0.00	56
	A	0.00	0.00	1.52	3.79	41.67	50.00	3.03	0.00	132
Cnn1-S74A-GFP	G1	0.00	0.00	1.12	13.48	52.81	24.72	7.87	0.00	89
	S	0.00	0.00	2.17	15.22	36.96	30.43	15.22	0.00	46
	M	0.00	0.00	1.02	11.22	36.22	31.12	15.31	5.10	196
	A	0.00	0.00	1.00	10.03	33.44	37.12	14.05	3.68	299
Cnn1-S74D-GFP	G1	0.00	0.00	1.89	18.87	35.85	24.53	16.98	1.89	58
	S	0.00	0.00	0.00	21.43	32.14	46.43	0.00	0.00	28
	M	0.00	0.00	2.63	17.54	28.07	34.21	14.91	2.63	114
	A	0.00	0.00	1.78	13.61	43.20	29.59	8.88	2.96	169
$Cnn1^{\Delta HFD}$-GFP	G1	46.00	0.00	2.00	6.00	30.00	16.00	0.00	0.00	50
	S	44.44	0.00	11.11	14.81	25.93	3.70	0.00	0.00	27
	M	41.35	0.75	4.51	9.77	24.81	15.79	3.01	0.00	113
	A	16.11	0.67	5.37	12.75	23.49	25.50	13.42	2.68	149
$Cnn1^{\Delta HFD}$-S74A-GFP	G1	51.92	0.00	1.92	9.62	17.31	19.23	0.00	0.00	52
	S	61.11	0.00	0.00	16.67	11.11	11.11	0.00	0.00	18
	M	37.98	1.55	2.33	8.53	31.01	16.28	2.33	0.00	129
	A	12.59	0.00	3.70	13.33	46.67	21.48	1.48	0.74	135
$Cnn1^{\Delta HFD}$-S74D-GFP	G1	100.00	0.00	0.00	0.00	0.00	0.00	0.00	0.00	n.a.[c]
	S	100.00	0.00	0.00	0.00	0.00	0.00	0.00	0.00	
	M	100.00	0.00	0.00	0.00	0.00	0.00	0.00	0.00	
	A	100.00	0.00	0.00	0.00	0.00	0.00	0.00	0.00	

n.a.; not applicable

[a] Intensity ratio of Cnn1-GFP to Spc110-mCherry – each intensity range represents the percentage of cells falling within that range.

[b] Number of cells counted for each cell cycle stage

[c] n.a. No GFP signal was detected at any cell cycle stage